arXiv:1404.7040v1 [cond-mat.mes-hall] 28 Apr 2014

Optical properties of magnetically doped ultra-thin topological insulator slabs.

Martha Lasia and Luis Brey
Instituto de Ciencia de Materiales de Madrid, (CSIC), Cantoblanco, 28049 Madrid, Spain
(Dated: April 29, 2014)

Starting from a three dimensional Hamiltonian, we study the optical properties of ultra-thin topological insulator slabs for which the coupling between Dirac fermions on opposite surfaces results in two degenerated gapped hyperbolic bands. The gap is a threshold for the optical absorption and translates in a peak in the imaginary part of the optical conductivity. An exchange field applied perpendicular to the slab splits the degenerated hyperbolic bands and a double step structure come out in the optical absorption, whereas a double peak structure appears in the imaginary part of the longitudinal optical conductivity. The exchange field breaks time-reversal symmetry and for exchange fields larger than the surfaces coupling gap, the zero frequency Hall conductivity is quantized to e^2/h. This result implies large values of the Kerr and Faraday rotation angles. In ultra-thin slabs, the absence of light multiple scattering and bulk conductivity, makes the Kerr and Faradays angles to remain rather large in a wide range of frequencies.

PACS numbers: 72.25.Dc,73.20.-r,73.50.-h

I. INTRODUCTION.

Three dimensional (3D) topological insulators (TI's) are materials that possess conducting metallic surface states in the bulk energy gap[1–3]. These systems typically are band insulators where strong spin orbit coupling alters the natural order in energies of the band structure. At the surface of the TI, in contact with the vacuum, the bands turn back to their natural order, and a two-dimensional metallic state merges at the surface. These surface states have an helical linear dispersion and the quasiparticles are governed by a two-dimensional (2D) massless Dirac equation. The Dirac cone is centered at a time reversal invariant point in the two dimensional Brillouin zone, and the degeneracy at the Dirac point is preserved by time reversal symmetry.

At zero temperature the optical conductivity of a system described by the two-dimensional Dirac Hamiltonian, with the chemical potential located at the Dirac point, gets a universal value of $\sigma_0=\frac{\pi}{2}\frac{e^2}{h}$. Light transmittance experiments have confirmed this universal value for the optical absorption in graphene[4, 5]. The optical properties of TI surface states has been theoretically studied recently[6–9], and the same universal value for the optical conductivity, σ_0, has been obtained[8, 9]. However, hexagonal warping terms to appear in the surface band structure of TI's modify the interband optical transition and deviations from the universal background as seen in graphene[4, 5] have been predicted[6, 7]. The optical conductivity of Bismuth based topological insulators has been experimentally studied[10–13], and the main result is that the exotic properties of the TI surface states are masked by high carrier densities and impurity band conduction.

The magnetoelectric coupling that occurs at the surfaces of topological insulators[1–3] is the origin of new and exotic phenomena such as the possibility of inducing magnetic monopoles[14], the tunable Casimir effect[15] and the giant magneto-optical Kerr and Faraday effects[16–21]. The Kerr and Faraday effects describe the rotation of the light polarization when it is reflected or transmitted respectively by a magnetic material. When time-reversal symmetry is broken at the surface of a TI, a gap is induced in the Dirac band structure and the surface shows an anomalous Hall effect, $\sigma_{xy}=\frac{1}{2}e^2/\hbar$. In this situation TI surfaces[16, 17] or a clean thin slabs[18, 19] will have a strong magnetoelectric effect that manifests, in ideal systems, in a universal Faraday rotation and a giant Kerr rotation. At the surfaces of TI's the time reversal symmetry can be broken without applying external magnetic fields. Doping the system with magnetic impurities induces an exchange field acting on the TI surface state[22]. Experiments in Bi_2Se_3 thin films indicate the existence of colossal Kerr[23] and Faraday[24] rotations in the THz regime when time reversal symmetry is broken by a strong magnetic field perpendicular to the slab.

Topological insulators as Bi_2Te_3, Bi_2Se_3 and (BiSb)Te, have a layered structure consisting of stacked quintuple layers with relatively weak coupling between them. Therefore, it is possible to prepare these crystals in the form of thin films. In thin films the bulk contribution to electrical conductivity and optical absorption can be reduced considerably, and these systems can be the appropriated geometry to observe surface properties of TI's[22, 25, 26]. When the thickness of the thin film is of the order of the surface-state decay length into the bulk ($\sim$ 10nm), the tunneling between the top and bottom surfaces opens an energy gap and two degenerate massive Dirac bands appear[27–30]. By increasing the layer thickness the gap decreases and oscillates and the system alternates between a trivial topological phase and a 2D quantum spin Hall topological phase. The existence of this gap indicates that the ultra-thin film behaves as a quasi 2D system, and not as a couple of 2D electron gases separated by a dielectric.

In this work we study the electrical and optical properties of ultra-thin TI slabs in presence of an exchange

field. Starting form a realistic 4×4 $\mathbf{k}\cdot\mathbf{p}$ Hamiltonian we compute the band structure and optical conductivity of TI slabs. The utilization of a realistic bulk Hamiltonian as the starting point releases the use of an momentum or energy cutoff in the calculations. Also, by starting from the 3D Hamiltonian, the surface states dispersion contains automatically quadratic momentum terms and electron hole asymmetry. We study the competition between the confining gap due to the coupling between states on opposite surfaces and the gap induced by the exchange field. Using the Kubo formula we calculate the optical conductivity of the TI slab. The longitudinal conductivity gives information of the optical absorption of the slab, whereas the zero frequency Hall conductivity indicates the topological character of the system. From the optical conductivity we obtain the Kerr and Faraday angles of a ultra thin TI slab. We obtain a giant Kerr angle and a quantized Faraday angle. Both angles get large values in a wide window of low frequencies and because the ultra-thin slab behaves as a 2D system they are not affected by TI bulk conductivity or by multiple reflection inside the TI slab.

II. BULK HAMILTONIAN

The low energy band structure of three dimensional topological insulators in the Bi_2Se_3 family of materials can be described by a four band Hamiltonian proposed by Zhang *et al.* [31, 32]. In the $\mathbf{k}\cdot\mathbf{p}$ formalism, states near zero energy and long wavelength are governed by a Hamiltonian of the form

$$H^{3D} = E(\mathbf{k}) + \begin{pmatrix} \mathcal{M}(\mathbf{k}) & A_1k_z & 0 & A_2k_- \\ A_1k_z & -\mathcal{M}(\mathbf{k}) & A_2k_- & 0 \\ 0 & A_2k_+ & \mathcal{M}(\mathbf{k}) & -A_1k_z \\ A_2k_+ & 0 & -A_1k_z & -\mathcal{M}(\mathbf{k}) \end{pmatrix}, \tag{1}$$

where $\mathcal{M}(\mathbf{k})=M_0-B_2(k_x^2+k_y^2)-B_1k_z^2$, $k_\pm=k_x\pm ik_y$ and $E(\mathbf{k})=C+D_1k_z^2+D_2(k_x^2+k_y^2)$. The four basis states for which this Hamiltonian is written are $|1>=|p1_z^+,\uparrow>$, $|2>=-i|p2_z^-,\uparrow>$,$|3>=|p1_z^+,\downarrow>$, and $|4>=i|p2_z^-,\downarrow>$, which are hybridized states of the Se p orbitals and the Bi p orbitals, with the superscripts $(\pm)$ standing for even and odd parity, and $\uparrow$ and $\downarrow$ for spin up and down respectively. The Hamiltonian parameters for a particular material can be obtained by fitting to density functional band structure calculations [32]. In the case of Bi_2Se_3 the relevant parameters are M_0=0.28eV, A_1=2.2$eV\mathring{A}$, A_2=4.1$eV\mathring{A}$, B_1=10$eV\mathring{A}^2$, B_2=56.6$eV\mathring{A}^2$, C=-0.0068eV, D_1=1.3$eV\mathring{A}^2$ and D_2=19.6$eV\mathring{A}^2$.

A. Electronic Structure of Topological Insulator Slabs.

We analyze a TI slab perpendicular to the z-direction and thickness L . The system is invariant in the (x,y)-plane so that k_x and k_y are good quantum numbers.

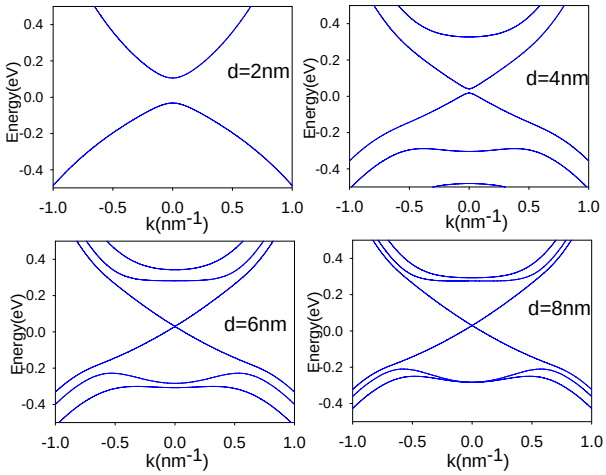

FIG. 1: (Color online) Band structure of TI slabs of different thickness d. The slabs are perpendicular to the $\hat{z}$ direction. The electronic sates are obtained by diagonalizing Hamiltonian Eq. 1 with the appropriated boundary conditions. At the Brillouin zone center, Γ, the bulk gap has a value $2M_0$=0.56eV. Energies inside the bulk energy gap correspond to surface states. For thick slabs low energy surface states dispersion has the form of a Dirac-cone. For thin slabs, coupling between surface states located on opposite surfaces opens an energy gap in the Dirac spectrum. The system has circular symmetry and we plot the bands as function of the absolute value of the in-plane wavevector $\mathbf{k}$.

The eigenvalues, $\varepsilon_{n,\mathbf{k}}$, and wavefunctions, $\Psi_{n,\mathbf{k}}(z)$, are obtained by solving Eq.1 with $k_z=-i\partial_z$ and forcing the wavefunction to vanish at the surfaces of the slab, $z=0$ and $z=L$. This is satisfied expanding $\Psi_{n,\mathbf{k}}(z)$ in harmonics, of the form $\sin\left(\frac{l}{L}\pi z\right)$, being l a positive integer[33]. For a given two-dimensional wavevector, $\mathbf{k}$ $=(k_x,k_y)$, we diagonalize the Hamiltonian in this basis and we obtain a discrete number of eigenvalues, $\varepsilon_{n,\mathbf{k}}$ and the corresponding wavefunctions,

$$\Psi_{n,\mathbf{k}}(z) = \frac{e^{i\mathbf{kr}}}{\sqrt{A}}\sqrt{\frac{2}{L}}\sum_{l=1}^{N_{\max}}\sum_{j=1,4} a_{n,j}^l(\mathbf{k})\sin\left(l\pi\frac{z}{L}\right)|j>, \tag{2}$$

here A is the sample area. The number of harmonics used in the expansion, N_{max}, depends on the thickness of the slab, and it is chosen large enough so that the results do not depend on its value.

In Fig.1 we plot the band structure of thin TI slabs for different values of the thickness d. For thick TI slabs ($d>6nm$) the surfaces are practically decoupled and two degenerated gapless Dirac-like bands, one for each surface, appear in the bulk energy gap region. This is the benchmark of the TI. As the thickness of the slab decreases the electronic states localized on opposite surfaces couple and the Dirac cones transform in two degenerated hyperbolic Dirac bands with gap E_g at the center of the Brillouin zone Γ. In agreement with previous works[27–30] the values of this gap oscillates as function of the

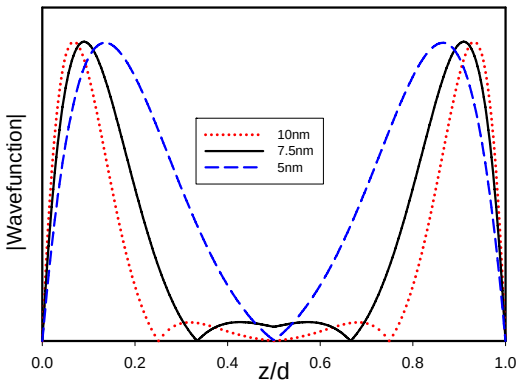

FIG. 2: (Color online) Absolute value of the wavefunction, as function of the position along the slab, of a surface state with momentum close to zero, for different TI slab thickness.

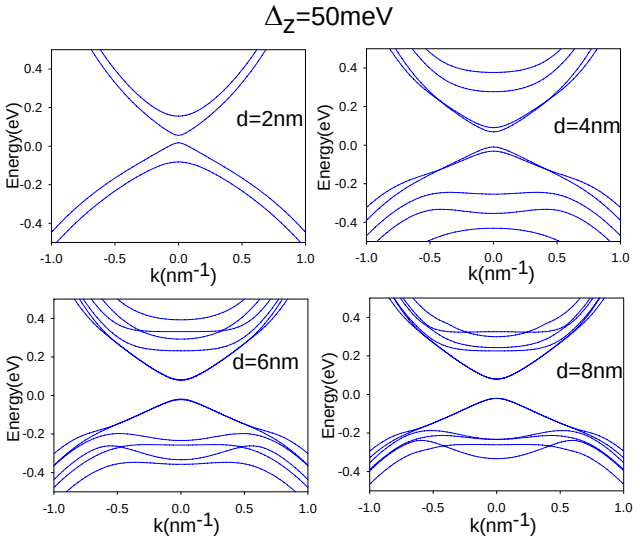

FIG. 3: (Color online) Band structure of TI slabs of different thickness d, in presence of an exchange field, Δ_z=50meV, applied in the z-direction. The slabs are perpendicular to the $\hat{z}$ direction. The electronic sates are obtained by diagonalizing Hamiltonian Eq. 1 with the appropriated boundary conditions. The system has circular symmetry and we plot the bands as function of the absolute value of the in-plane wavevector **k**.

thickness d. For each set of gapped Dirac bands, the expectation value of the spin in the valence and conduction bands, gets a **k**-dependent configuration near the center of the Brillouin zone[29, 30]. Because of time reversal symmetry, the other pair of Dirac hyperbolas is a degenerated copy with the opposite **k**-dependent spin configuration[29, 30].

The energy gap for the Dirac fermions occurs when the thickness of the TI slab is comparable with the decay length of the surface state wave function into the film. In that case opposite surface wave functions overlap leading to the appearance of the energy gap at the center of the Brillouin zone. In Fig.2 we plot the absolute value of the wave function of a surface state with momentum close to zero for different values of the layer thickness. If we turn the parameters D_1 and D_2 to zero, it is possible to obtain analytically that the four components of the surface wavefunction have the same dependence on the position across the TI slab,

$$f(z) = e^{\lambda_1 z} \sin \lambda_2 z \tag{3}$$

with

$$\lambda_1 + i\lambda_2 = \frac{A_1 + i\sqrt{|A_1^2 - 4M_0 B_1|}}{2B_1} \ . \tag{4}$$

From the Bi_2Se_3 band structure parameters we get $\lambda_1 \sim 1.1nm^{-1}$ and $\lambda_2 \sim 1.26nm^{-1}$ in rather good agreement with the decays length and zeros of the wavefunction in Fig.2. From this values of the decay length, we conclude that in TI slabs thinner than 6nm, there is coupling between top and bottom surfaces and the system can not be described as a couple of two-dimensional gases separated by a dielectric. It is more appropriated describe the TI slab as a 2D system.

B. Spectrum of a TI slabs in presence of a Exchange field.

An exchange field directed along the z-direction affects strongly the electronic properties of TI surfaces. The Dirac Hamiltonian describing electrons moving on a surface perpendicular to the z-direction has the form[32, 34] $H=\hbar v_F(\sigma_x k_y - \sigma_y k_x)$. Here the Pauli matrices σ_x and σ_y correspond to the electron spin operators and v_F is the Fermi velocity. An exchange field Δ_z pointing in the z-direction opens a gap in the surface bands and the system becomes a topological insulator showing a Hall conductivity $\sigma_{xy}=1/2e^2/h$. The presence of different oriented surfaces in real crystals, makes that measured Hall conductances become always integrally quantized[35–37].

We study the effect of a exchange field on the properties of a TI thin film, by adding to the bulk Hamiltonian Eq.1 a exchange term of the form $\Delta_Z I \otimes \sigma_z$. The slab geometry is introduced by forcing the wavefunctions to satisfy the boundary conditions, Eq.2. In Fig.3 we plot the band structure of thin TI slabs for different values of the thickness d and a typical exchange field Δ_z=50meV.

For thick slabs where opposite surfaces are decoupled, the exchange field polarizes, near **k**=0, the spin of the conduction(valence) band in the +(−) z-direction. Then a gap of magnitude $2\Delta_z$ appears and the bands get a quadratic dispersion. Away from the center of the Brillouin zone, the bands recover the linear dispersion and the spin texture dictated by the Dirac equation is re-

stored.

At Δ_z=0, ultra thin TI slabs have two degenerated hyperbolic Dirac bands with opposite spin texture. The exchange field breaks the time reversal symmetry, and near $\mathbf{k}$=0 the bands split in two states with spin up and energies $\pm E_g/2+\Delta_z$ and two spin down states with energies $\pm E_g/2-\Delta_z$.

III. OPTICAL CONDUCTIVITY

The optical conductivity $\sigma_{\alpha,\beta}$ relates, in the linear response, the electrical current in a direction α to an external transverse electric field applied in the β-direction.

The optical conductivity consists of two pieces, the diamagnetic term and the paramagnetic term[38]. The paramagnetic term can be obtained from the current-current correlation function using the Kubo formalism. However the diamagnetic term is not always well described in continuos effective models. In particular, in the Dirac Hamiltonian the diamagnetic term vanishes because $\partial^2 H/\partial k^2$=0 [39, 40].

Both the diamagnetic and paramagnetic contributions contains a delta singularity at frequency ω=0. The total weight of the delta is the Drude weight or charge stiffness and indicates the ability of the carriers to move freely when an electric field is applied. In this work we are considering undoped systems with no carriers at the Fermi energy and therefore the delta function should have null weight. To achieve this, we use the following expression[41] for the optical conductivity that cancels the delta singularity at ω=0, and guarantees a zero charge stiffness in the systems,

$$\sigma_{\alpha,\beta}(\omega)=i\frac{e^2\hbar}{V}\int\frac{d^2\mathbf{k}}{(2\pi)^2}\sum_{m,n}\frac{n_F(\varepsilon_{n,\mathbf{k}})-n_F(\varepsilon_{m,\mathbf{k}})}{\varepsilon_{m,\mathbf{k}}-\varepsilon_{n,\mathbf{k}}}\frac{<n,\mathbf{k}|j_\alpha|m,\mathbf{k}><m,\mathbf{k}|j_\beta|n,\mathbf{k}>}{\hbar(\omega+i\eta)-(\varepsilon_{m,\mathbf{k}}-\varepsilon_{n,\mathbf{k}})} \tag{5}$$

In this expression $|m,\mathbf{k}>$ and $\varepsilon_{m,\mathbf{k}}$ are the eigenfunction and eigenvalues respectively of the system with subband m and wavevector $\mathbf{k}$, n_F is the fermi occupation, and $\hbar\eta$ represents the quasiparticle lifetime broadening. The current operators are obtained from the Hamiltonian through j_α=-$\partial H/\partial k_\alpha$.

Note that we do not need to include an energy cutoff in the calculation of the optical conductivity. The number of surface states is naturally limited by the bulk bands of the TI.

A. Zero exchange field.

For zero exchange field the system has time-reversal symmetry and the non-diagonal components of the conductivity tensor are zero. Also because of the circular symmetry of the Hamiltonian the system is isotropic and σ_{xx}=σ_{yy}. In Fig.4 we show the optical conductivity as a function of frequency for TI slabs of different thickness.

We first discuss the optical conductivity of uncoupled surfaces. In the insets of Fig.4 we plot the conductivity for a layer thickness d=20nm. For this thickness electronic states of both surfaces are decoupled and the dispersion near the center of the Brillouin zone is linear. Then at small ω, the imaginary part of the optical absorption is zero and the real part gets the value σ_0=$\frac{\pi}{4}\frac{e^2}{h}$. The value of σ_0 is half the value of the optical conductivity of graphene monolayer[42, 43], because although there is a Dirac cone at each surface, they are not spin degenerated. At frequencies near 0.35eV the dispersion relation deviates from the linear behavior and the real part of the conductivity increases continuously with ω and presents a strong peak at the TI energy gap. The imaginary part increases continuously from zero and presents a peak valley structure at the bulk energy gap.

At smaller layer thickness the coupling between opposite surface states opens a gap that suppress the optical absorption at frequencies smaller than the gap. At $\hbar\omega$=E_g, the hyperbolic dispersion and the modification of the spin texture near Γ increases the number of $\mathbf{k}$ states that participate in the transition and this produces a peak superposed to a step in the real part of σ_{xx}. As the gap reduces the step in Reσ_{xx} tends to σ_0 and the peak disappears. The gap, also induces a peak in the imaginary part of σ_{xx} which indicates the existence of an interband charge collective excitation.

B. Finite exchange field.

The exchange field breaks time reversal symmetry and the non-diagonal part of the optical conductivity gets a finite value. For thin gapped TI slabs, the exchange field polarizes the spin in the extremes of the bands, and the dissipative parts of the response functions, Reσ_{xx} and Imσ_{xy}, show two absorption edges at energies $2\Delta_z\pm E_g$. The splitting of the bands also reflects in the appearance of two peaks in Imσ_{xx} and Reσ_{xy}. At large separation between the surfaces only an absorption edge and a peak occur at energy $2\Delta_z$.

A TI slab in presence of a exchange field has always an insulator character. The band insulator or topological insulator nature of this phase may be known by com-

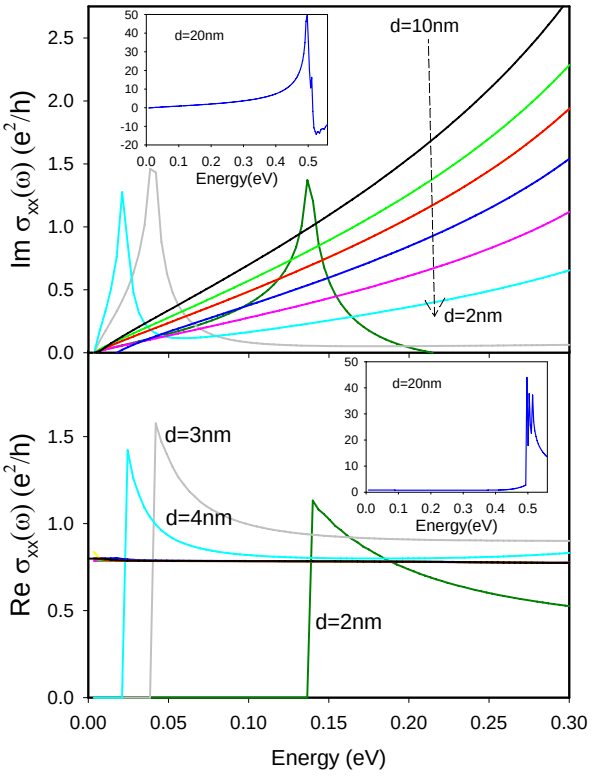

FIG. 4: (Color online) Imaginary (top) and real (bottom) part of the optical conductivity as a function of frequency, for a TI slab of different thicknesses. In the insets we show the optical conductivity for a thick slab, d=20nm with states in opposite surfaces practically decoupled

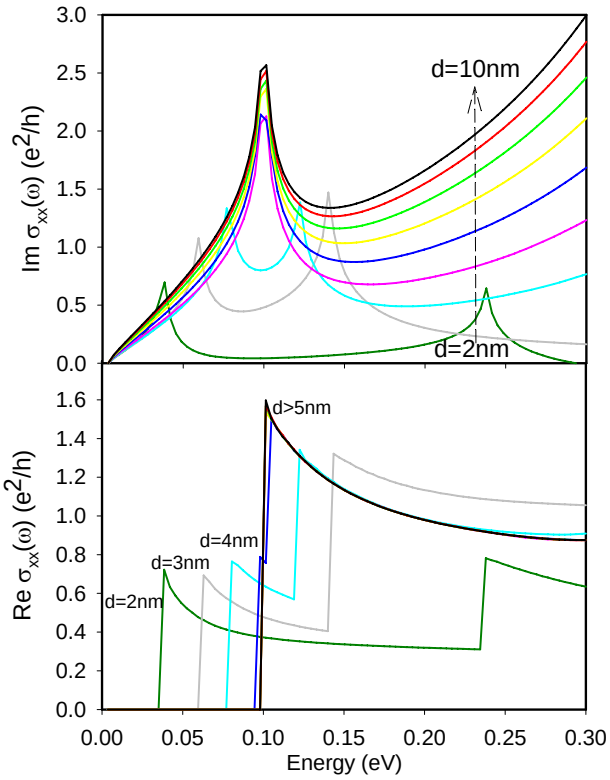

FIG. 5: (Color online) Imaginary (top) and real (bottom) part of the longitudinal optical conductivity as a function of frequency, for a TI slab of different thicknesses, in presence of an exchange field Δ_z=50meV.

puting the Chern number, which in this system[1, 44] coincides with the value of the dc Hall conductivity. In Fig.7 we plot the Hall conductivity as function of d and Δ_z. For values of the exchange field smaller than twice the tunneling gap, the slab is a normal insulator, however for larger values of Δ_Z, the TI slab acquires an integer anomalous Hall conductivity, σ_{xy}=e^2/h. Then as a function of the exchange field or the slab thickness, TI slabs undergo quantum phase transitions from band to topological insulator. The system only presents an anomalous quantum Hall effect when the surface bands are inverted by the exchange field, independently of the sign of the tunneling gap between the surfaces. For very large values of d, the integer quantized Hall conductivity may be understood as the sum of two half quantized Hall conductivities, one for each uncoupled surface.

IV. KERR AND FARADAY ANGLES.

Finite values of the Hall conductivity in magnetically gapped TI surfaces imply interesting properties in their optical properties. When $\sigma_{xy} \neq 0$, left and right handed circularly polarized light, propagating perpendicular to the TI slab, have different refraction and transmission indices. As a consequence, linear polarized light rotates its polarization direction when transmitted or reflected by a TI slab in the anomalous quantum Hall regime. The transmitted and reflected rotation angles of linear polarized light are called Kerr (θ_K) and Faraday (θ_F) respectively.

Because of the overlap between electronic states localized on opposite surfaces, ultra thin TI slabs should be considered as a single two dimensional electron system. Furthermore, the light wavelength is much larger than the slab thickness and the light electromagnetic fields are practically constants across the slab. In this situation, the electromagnetic properties of the thin TI slab are described just by the two dimensional conductivity tensor. Transmission and reflection of light are obtained by considering two dielectric materials separated by an interface characterized by a conductivity tensor.

Maxwell equations dictates the boundary conditions for the electromagnetic fields. For a free standing slab and normal incidence, the reflection, $\bar{r}$=$\begin{pmatrix} r_{xx} & r_{xy} \\ -r_{xy} & r_{xx} \end{pmatrix}$ and transmission, $\bar{t}$=$\begin{pmatrix} t_{xx} & t_{xy} \\ -t_{xy} & t_{xx} \end{pmatrix}$ tensors for the elec-

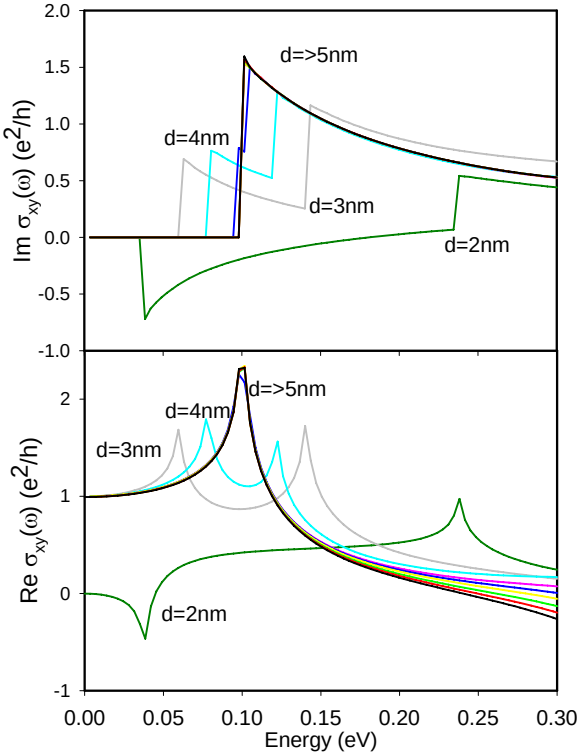

FIG. 6: (Color online) Imaginary (top) and real (bottom) part of the Hall optical conductivity as a function of frequency, for a TI slab of different thicknesses, in presence of an exchange field Δ_z=50meV.

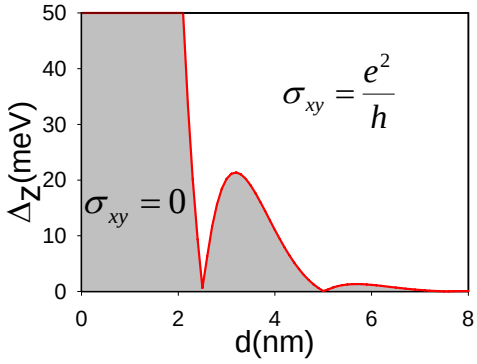

FIG. 7: (Color online) Phase diagram, as a function of d and Δ_z, for the anomalous quantum Hall effect of a TI slab perpendicular to the z-direction.

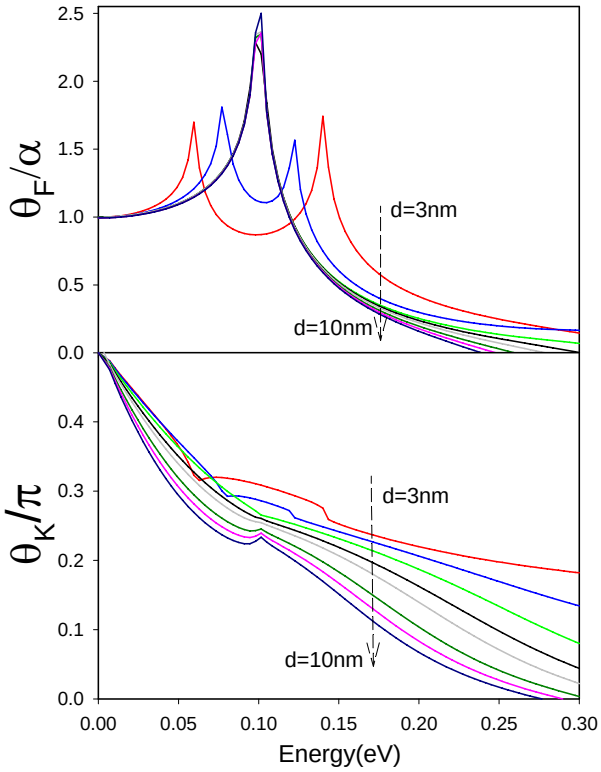

FIG. 8: (Color online) Faraday and Kerr angles for TI slabs of different thicknesses in presence of an exchange field Δ_z=50meV.

tric field have the form[19],

$$\begin{aligned} r_{xx} &= \frac{1-(1+\frac{4\pi}{c}\sigma_{xx})^2-(\frac{4\pi}{c}\sigma_{xy})^2}{(2+\frac{4\pi}{c}\sigma_{xx})^2+(\frac{4\pi}{c}\sigma_{xy})^2} \\ r_{xy} &= \frac{-\frac{8\pi}{c}\sigma_{xy}}{(2+\frac{4\pi}{c}\sigma_{xx})^2+(\frac{4\pi}{c}\sigma_{xy})^2} \\ t_{xx} &= \frac{4+\frac{8\pi}{c}\sigma_{xx}}{(2+\frac{4\pi}{c}\sigma_{xx})^2+(\frac{4\pi}{c}\sigma_{xy})^2} \\ t_{xy} &= \frac{-\frac{8\pi}{c}\sigma_{xy}}{(2+\frac{4\pi}{c}\sigma_{xx})^2+(\frac{4\pi}{c}\sigma_{xy})^2}\,. \end{aligned} \tag{6}$$

and the Kerr and Faraday angles are given by,

$$\begin{aligned} \theta_F &= \arg(t_{xx}+it_{xy}) \\ \theta_K &= \arg(r_{xx}+ir_{xy}) \end{aligned} \tag{7}$$

In Fig.8 we plot the Kerr and Faraday angles for TI slabs with thickness ranging from d=2nm to d=10nm, in presence of an exchange field Δ_z=50meV. For $\Delta_z \neq 0$, TI slabs exhibit anomalous quantum Hall effect characterized by $\sigma_{xx}(\omega=0)$=0, Re$\sigma_{xy}(\omega=0)$=0 and Im$\sigma_{xy}(\omega=0)$=e^2/h, then the Kerr angle, Eq.6, gets a large (giant) value θ_K=-$\pi/2$ and the Faraday gets a quantized value θ_F=α, being α=$e^2/\hbar c$=1/137 the vacuum fine structure

constant[18, 19]. Absolute values of both angles decay with frequency and present peaks at the optical absorption edges ω=$2\Delta_z \pm E_g$.

The results indicate that in a wide range of frequencies, linear polarized light gets a large rotation in its polarization when reflected or transmitted by an ultra thin TI slab. The small value of the slab thickness makes this result rather robust. For ultra-thin TI slabs the bulk contribution to the electronic conductivity is totally suppressed and the values of θ_K and θ_F are not affected by bulk free carriers supply by bulk defects. Also because the thickness of the slab is much smaller than the light wavelength, the optical path of the light inside the TI slab is zero and there is not suppression of θ_K and θ_F by multiple reflections in side the TI slab. We then conclude that in ultra-thin TI slabs there is a wide range of frequencies where the Kerr and Faraday angles get large values.

V. CONCLUSIONS.

We have studied the band structure and optical properties of ultra-thin topological insulator slabs. The electronic properties are obtained starting from a three-dimensional $\mathbf{k} \cdot \mathbf{p}$ Hamiltonian, so that our calculations do not depend on energy or momentum cutoff. For the optical conductivity we use an expression (Eq.5) that describes correctly both the diamagnetic and the paramagnetic contributions, and therefore we obtain the real and imaginary part of the conductivity directly from it.

In thin TI slabs, the coupling between opposite surface states opens a gap in the electronic spectrum that inhibits optical absorption for frequencies smaller than the gap E_g. The gap also reflects in a peak at $\hbar\omega$=E_g in the imaginary part of $\sigma_{xx}(\omega)$. This peak indicates the existence of an interband charge excitation.

An exchange field Δ_z applied perpendicularly to the TI slab, breaks time-revesal symmetry and splits the gapped bands of ultra-thin TI slabs. The real part of the longitudinal optical conductivity shows absorption edges at energies $2\Delta_z \pm E_g$, whereas the imaginary part presents peaks at the same energies. For values of the exchange field $2\Delta_z > E_g$, the zero frequency Hall conductivity is quantized to the value σ_{xy}=e^2/h. This large value of the Hall conductivity produces a strong rotation of the polarization of light when transmited through or reflected in the TI slab. At zero frequency the Faraday angle gets the value θ_F=$e^2/\hbar c$=1/137 and presents peaks at frequencies $2\Delta_z \pm E_g$. The Kerr rotation gets a value θ_K=-$\pi/2$ at zero frequency and gets rather large absolute values at finite frequencies. These values of the Faraday and Kerr rotation angles are rather robust because they are not affectd by bulk carriers or by light multiple scattering in the topological insulator ultra-thin slab.

VI. ACKNOWLEDGMENTS.

Funding for this work was provided by MEC-Spain via grant FIS2012-33521.

[1] M. Z. Hasan and C. L. Kane, Rev. Mod. Phys. **82**, 3045 (2010).

[2] X.-L. Qi and S.-C. Zhang, Rev. Mod. Phys. **83**, 1057 (2011).

[3] Y. Ando, ArXiv e-prints (2013), 1304.5693.

[4] R. R. Nair, P. Blake, A. N. Grigorenko, K. S. Novoselov, T. J. Booth, T. Stauber, N. M. R. Peres, and A. K. Geim, Science **320**, 1308 (2008), http://www.sciencemag.org/content/320/5881/1308.full.pdf, URL `http://www.sciencemag.org/content/320/5881/1308.abstract`.

[5] T. Stauber, N. M. R. Peres, and A. K. Geim, Phys. Rev. B **78**, 085432 (2008), URL `http://link.aps.org/doi/10.1103/PhysRevB.78.085432`.

[6] Z. Li and J. P. Carbotte, Phys. Rev. B **87**, 155416 (2013), URL `http://link.aps.org/doi/10.1103/PhysRevB.87.155416`.

[7] X. Xiao and W. Wen, Phys. Rev. B **88**, 045442 (2013), URL `http://link.aps.org/doi/10.1103/PhysRevB.88.045442`.

[8] D. Schmeltzer and K. Ziegler, ArXiv e-prints (2013), 1302.4145.

[9] N.M.Peres and J. E.Santos, Journal of Physics: Condensed Matter **25**, 305801 (2013).

[10] A. D. LaForge, A. Frenzel, B. C. Pursley, T. Lin, X. Liu, J. Shi, and D. N. Basov, Phys. Rev. B **81**, 125120 (2010), URL `http://link.aps.org/doi/10.1103/PhysRevB.81.125120`.

[11] P. Di Pietro, F. M. Vitucci, D. Nicoletti, L. Baldassarre, P. Calvani, R. Cava, Y. S. Hor, U. Schade, and S. Lupi, Phys. Rev. B **86**, 045439 (2012), URL `http://link.aps.org/doi/10.1103/PhysRevB.86.045439`.

[12] A. Akrap, M. Tran, A. Ubaldini, J. Teyssier, E. Giannini, D. van der Marel, P. Lerch, and C. C. Homes, Phys. Rev. B **86**, 235207 (2012), URL `http://link.aps.org/doi/10.1103/PhysRevB.86.235207`.

[13] K. W. Post, B. C. Chapler, L. He, X. Kou, K. L. Wang, and D. N. Basov, Phys. Rev. B **88**, 075121 (2013), URL `http://link.aps.org/doi/10.1103/PhysRevB.88.075121`.

[14] X.-L. Qi, R. Li, J. Zang, and S.-C. Zhang, Science **323**, 1184 (2009), http://www.sciencemag.org/content/323/5918/1184.full.pdf, URL `http://www.sciencemag.org/content/323/5918/1184.abstract`.

[15] A. G. Grushin and A. Cortijo, Phys. Rev. Lett. **106**, 020403 (2011), URL `http://link.aps.org/doi/10.1103/PhysRevLett.106.020403`.

[16] X.-L. Qi, T. L. Hughes, and S.-C. Zhang, Phys. Rev. B **78**, 195424 (2008), URL `http://link.aps.org/doi/10.1103/PhysRevB.78.195424`.

[17] A. M. Essin, J. E. Moore, and D. Vanderbilt, Phys. Rev. Lett. **102**, 146805 (2009), URL `http://link.aps.org/doi/10.1103/PhysRevLett.102.146805`.

[18] W.-K. Tse and A. H. MacDonald, Phys. Rev. Lett. **105**, 057401 (2010), URL http://link.aps.org/doi/10.1103/PhysRevLett.105.057401.

[19] W.-K. Tse and A. H. MacDonald, Phys. Rev. B **84**, 205327 (2011), URL http://link.aps.org/doi/10.1103/PhysRevB.84.205327.

[20] A. Karch, Phys. Rev. Lett. **103**, 171601 (2009), URL http://link.aps.org/doi/10.1103/PhysRevLett.103.171601.

[21] M.-C. Chang and M.-F. Yang, Phys. Rev. B **80**, 113304 (2009), URL http://link.aps.org/doi/10.1103/PhysRevB.80.113304.

[22] C.-Z. Chang, J. Zhang, X. Feng, J. Shen, Z. Zhang, M. Guo, K. Li, Y. Ou, P. Wei, L.-L. Wang, et al., Science **340**, 167 (2013), http://www.sciencemag.org/content/340/6129/167.full.pdf, URL http://www.sciencemag.org/content/340/6129/167.abstract.

[23] R. Valdés Aguilar, A. V. Stier, W. Liu, L. S. Bilbro, D. K. George, N. Bansal, L. Wu, J. Cerne, A. G. Markelz, S. Oh, et al., Phys. Rev. Lett. **108**, 087403 (2012), URL http://link.aps.org/doi/10.1103/PhysRevLett.108.087403.

[24] G. S. Jenkins, A. B. Sushkov, D. C. Schmadel, M.-H. Kim, M. Brahlek, N. Bansal, S. Oh, and H. D. Drew, Phys. Rev. B **86**, 235133 (2012), URL http://link.aps.org/doi/10.1103/PhysRevB.86.235133.

[25] J. Wang, B. Lian, H. Zhang, and S.-C. Zhang, Phys. Rev. Lett. **111**, 086803 (2013), URL http://link.aps.org/doi/10.1103/PhysRevLett.111.086803.

[26] H.-Z. Lu, A. Zhao, and S.-Q. Shen, Phys. Rev. Lett. **111**, 146802 (2013), URL http://link.aps.org/doi/10.1103/PhysRevLett.111.146802.

[27] J. Linder, T. Yokoyama, and A. Sudbø, Phys. Rev. B **80**, 205401 (2009).

[28] Yi Zhang *et al.* , Nature Physics **6**, 584 (2010).

[29] H.-Z. Lu, W.-Y. Shan, W. Yao, Q. Niu, and S.-Q. Shen, Phys. Rev. B **81**, 115407 (2010).

[30] C.-X. Liu, H. Zhang, B. Yan, X.-L. Qi, T. Frauenheim, X. Dai, Z. Fang, and S.-C. Zhang, Phys. Rev. B **81**, 041307 (2010).

[31] H. Zhang, *et al.*, Nature Phys. **5**, 438 (2009).

[32] C.-X. Liu, X.-L. Qi, H. Zhang, X. Dai, Z. Fang, and S.-C. Zhang, Phys. Rev. B **82**, 045122 (2010).

[33] M. Lasia and L. Brey, Phys. Rev. B **86**, 045317 (2012), URL http://link.aps.org/doi/10.1103/PhysRevB.86.045317.

[34] P. G. Silvestrov, P. W. Brouwer, and E. G. Mishchenko, Phys. Rev. B **86**, 075302 (2012), URL http://link.aps.org/doi/10.1103/PhysRevB.86.075302.

[35] D.-H. Lee, Phys. Rev. Lett. **103**, 196804 (2009), URL http://link.aps.org/doi/10.1103/PhysRevLett.103.196804.

[36] O. Vafek, Phys. Rev. B **84**, 245417 (2011), URL http://link.aps.org/doi/10.1103/PhysRevB.84.245417.

[37] L. Brey and H. A. Fertig, Phys. Rev. B **89**, 085305 (2014), URL http://link.aps.org/doi/10.1103/PhysRevB.89.085305.

[38] G. Giuliani and G. Vignale, *Quantum Theory of the Electron Liquid* (Cambridge University Press, 2005), 1st ed.

[39] T. Stauber and G. Gómez-Santos, Phys. Rev. B **82**, 155412 (2010), URL http://link.aps.org/doi/10.1103/PhysRevB.82.155412.

[40] T. Stauber, P. San-Jose, and L. Brey, New Journal of Physics **15**, 113050 (2013).

[41] P. B. Allen, *Conceptual Foundations of Material Properties: A standard model for calculation of ground and excited state properties.* (M.L.Cohen and S.G.Loiiue Eds. Elsevier, Amsterdam, 2006).

[42] V. P. Gusynin, S. G. Sharapov, and J. P. Carbotte, Phys. Rev. B **75**, 165407 (2007), URL http://link.aps.org/doi/10.1103/PhysRevB.75.165407.

[43] S. H. Abedinpour, G. Vignale, A. Principi, M. Polini, W.-K. Tse, and A. H. MacDonald, Phys. Rev. B **84**, 045429 (2011), URL http://link.aps.org/doi/10.1103/PhysRevB.84.045429.

[44] E. Prada, P. San-Jose, L. Brey, and H. Fertig, Solid State Communications **151**, 1075 (2011).